frontiers in Energy Research

ORIGINAL RESEARCH
published: 03 August 2021
doi: 10.3389/fenrg.2021.699879

Risk Analysis of Voltage Violation With PHEV Inter-Area Mobile Charging Strategy Under Gas Station Networks Attacked

Xue Li, Zhourong Zhang and Dajun Du**

Shanghai Key Laboratory of Power Station Automation Technology, School of Mechatronic Engineering and Automation, Shanghai University, Shanghai, China

To reduce the risk of voltage violation after gas station networks (GSNs) are attacked, this study investigates an inter-area mobile charging strategy of plug-in hybrid electric vehicles (PHEVs) to decrease the charging load by taking full advantage of charging resources. First, considering the location of the charging station, the waiting time, and the charging fee, an inter-area mobile charging strategy of PHEVs is proposed, and a mobile charging model of PHEVs among regions is established to relieve the charging pressure. Second, the risk index is developed to analyze the risk of voltage violation in terms of the results of probabilistic load flow (PLF). Finally, the proposed strategy is tested on a modified coastal active power distribution network, and simulation results show that the charging load of PHEVs is dispersed among regions and the risk of voltage over-limit can be reduced.

Keywords: gas station network (GSN), attack, plug-hybrid electric vehicle (PHEV), mobile charging strategy, risk of voltage violation

OPEN ACCESS

Edited by:
Zhile Yang,
Shenzhen Institutes of Advanced Technology (CAS), China

Reviewed by:
Yuanjun Guo,
Shenzhen Institutes of Advanced Technology (CAS), China
Yanhui Zhnag,
Shenzhen Institutes of Advanced Technology (CAS), China
Tingli Chemg,
Hefei University of Technology, China

****Correspondence:***
Zhourong Zhang
rong41188@163.com
Dajun Du
ddj@i.shu.edu.cn

Specialty section:
This article was submitted to Electrochemical Energy Conversion and Storage, a section of the journal Frontiers in Energy Research

Received: *24 April 2021*
Accepted: *24 June 2021*
Published: *03 August 2021*

Citation:
Li X, Zhang Z and Du D (2021) Risk Analysis of Voltage Violation With PHEV Inter-Area Mobile Charging Strategy Under Gas Station Networks Attacked. Front. Energy Res. 9:699879. doi: 10.3389/fenrg.2021.699879

1 INTRODUCTION

The scale of plug-in hybrid electric vehicles (PHEVs) has developed rapidly during the past several years. The high penetration of PHEVs causes the power grids to confront the operation risks (Badawy and Sozer (2017)). Moreover, with the increasing pervasion of communication networks into gas stations, gas station networks (GSNs) have been formed (Chao et al. (2018); Xie et al. (2018); Zhang et al. (2019); Du et al. (2019a)), which are also subject to cyberattacks. Once GSNs are attacked, the charging load will definitely increase with the lack of fuel in PHEVs. Due to the limited number of charging piles, it is an indisputable fact that charging resources will be scarce under GSNs that have been attacked. The increasing of the charging load can raise the voltage violation risks of grids (Li et al. (2020)). It is necessary to investigate the charging strategy of PHEVs to allocate the charging resources reasonably and the grid voltage violation risk to guarantee the safe operation of power grids.

Various charging strategies have been proposed to deal with the problems mentioned above that are caused by the PHEV charging load. Vehicle-to-grid (V2G) strategies are developed (Ko et al. (2018); Liu D. et al. (2018); Zhong et al. (2018); Zeng et al. (2018)). A battery replacement strategy has been proposed (Dong et al. (2016)), which cannot reduce the charging demand under GSNs that have been attacked. A centralized charging strategy of PHEVs has been presented to reduce voltage deviation *via* a series of fitness functions (Maigha and Mariesa Crow, (2014)). A PHEV smart charging strategy has been proposed to minimize the MG dependency on the main grid (Fouladi et al. (2019)). An orderly charging strategy has been investigated by considering various factors such as the

economic benefits of users (Liu A. et al. (2018)), the working status of charging piles and charging habits of users (Chen and Huang (2019)), the fluctuation of the charging load (Cai et al. (2021)), and so on. However, the surge of the PHEV charging load will lead to a long queue in the charging stations of GSNs' attacked areas, while the public charging piles in the unattacked area may be in an idle status, as shown in **Figure 1**. In this regard, the strategies mentioned above are not applicable without investigating the charging optimization among the areas. Moreover, the queuing problem in charging stations is rarely considered.

It is undeniable that the increase in the PHEV charging load in the attacked area will bring another problem, in that the security of the grid operation will be damaged. Various negative effects of electric vehicles connecting to the power grid are investigated, including voltage risks, and power flow risks (Pouladi et al. (2016); Salehi and Abdolahi (2019); Nafisi et al. (2016a); Yang et al. (2020); Wang et al. (2018); Nornagoro et al. (2020)). The impact of electric vehicle access on the voltage drops and power loss of power grids has been analyzed without establishing a relevant index (Pouladi et al. (2016); Salehi and Abdolahi (2019); Nafisi et al. (2016a)). The voltage over-limit and overload risk caused by electric vehicles connecting to the power grid have been presented from the perspective of components and networks (Yang et al. (2020)). The risks caused by the charging and discharging of electric vehicles to microgrids have been evaluated, from the aspects of expected lack of power supply, expected load reduction frequency, and load reduction probability (Wang et al. (2018)). The load loss ratio and overload risks are analyzed (Li et al. (2021); Du et al. (2019b)). The studies mentioned above only focus on the impact on the voltage level of power grids under the normal operation of GSNs. Even so, the risks are seldom quantified (Pouladi et al. (2016); Salehi and Abdolahi (2019); Nafisi et al. (2016a)). Due to the coincidence of the charging peak of the electric vehicle and the daily load peak (Nafisi et al. (2016b)), the surge of the PHEV charging load in the attacked area could greatly reduce the grid voltage, especially during the peak charging period.

To address these problems under GSNs that have been attacked, this study analyzes the risk of voltage violation while using a mobile charging strategy of regional PHEVs. The main contributions of this study are as follows:

1) Considering the location of charging stations, waiting time, and charging fee, an inter-area mobile charging strategy of PHEVs is proposed to choose the optimal charging station. A PHEV mobile charging model is then established to disperse the charging stress in the attacked region.

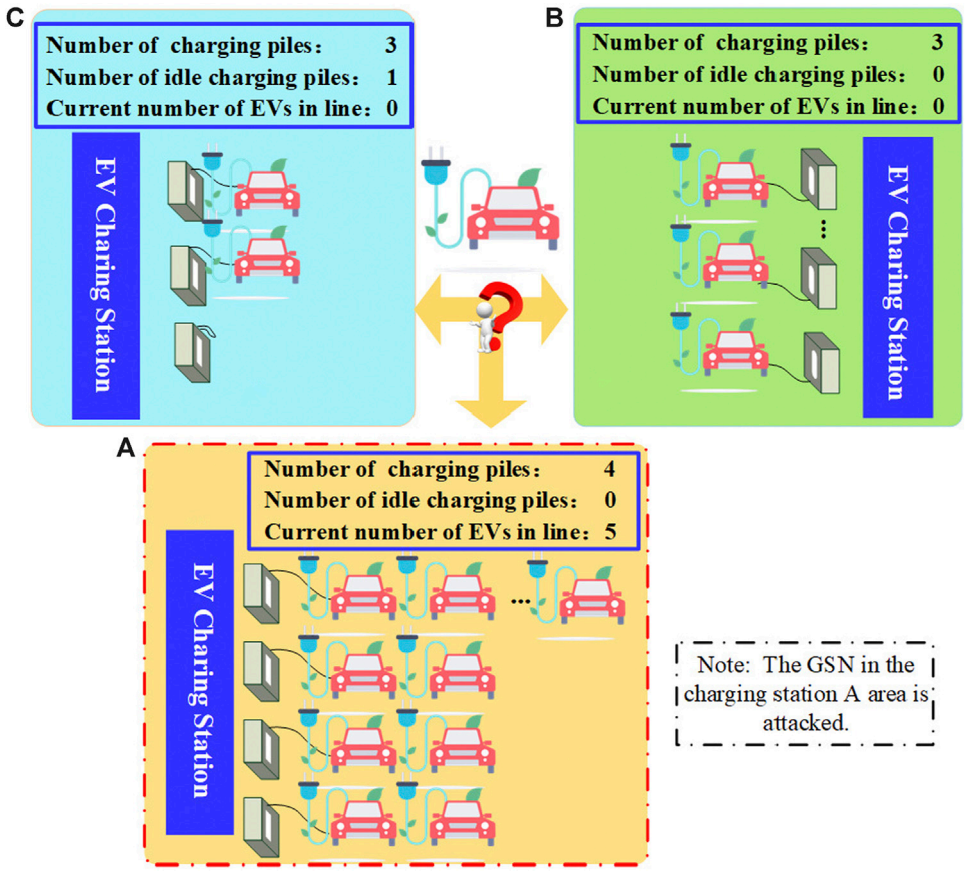

FIGURE 1 | Schematic diagram of the unbalanced charging load.

2) Considering the probability and severity of voltage violation, an index of the voltage violation risk is developed to analyze the impact of PHEV mobile charging on distribution networks under GSNs' attacked regions.

The rest of this article is organized as follows. **Section 2** describes the PHEV mobile charging model based on the mobile charging strategy, including the PHEV charging model and the queue charging model. **Section 3** presents the index of the voltage violation risk based on the results of probabilistic load flow (PLF). In **section 4**, simulation results are shown in detail, followed by discussion in **section 5**.

2 PROBABILITY MODEL OF PLUG-IN HYBRID ELECTRIC VEHICLE MOBILE CHARGING

The driving mode of PHEVs can be divided into the combustion mode and the electric mode depending on different driven powers. In the traditional charging model of PHEVs, the electric energy required to charge is determined by the daily driving distance and operating status (OS). The OS is the ratio of the distance traveled in the electric mode to the daily driving mileage. Once GSNs are attacked, the PHEV will be more dependent on the electric power, as presented in **Figure 2**. Moreover, the length of queuing in the charging stations may be longer due to the limitation of charging piles.

To solve the problem mentioned above, a mobile charging strategy is designed by considering the queue length, the charging fee, and the geographical location of each charging station. Then, the PHEV mobile charging model is established based on the mobile charging strategy.

2.1 Mobile Charging Strategy of Plug-In Hybrid Electric Vehicles With Gas Station Networks Attacked

Due to the limited number of charging piles, it is undeniable that there will be a charging congestion in charging stations located in GSNs' attacked areas, while there are some charging piles available in other charging stations. In this regard, this section proposes a mobile charging strategy for PHEVs between regions by considering charging fee, moving distance, and queuing time, as shown in **Figure 3**.

First, the expected charging fees for the i^{th} PHEV in different charging stations need to be calculated as follows:

$$Q^i = \frac{E^i}{\kappa^i} \times c_{station}, \tag{1}$$

where $c_{station}$ is the charging unit price, E^i is the power required to fully charge the i^{th} PHEV, and κ^i is the charging efficiency. Charging unit prices of different charging stations vary due to the station scales, electricity prices, and so on. It should be noted that the charging unit prices are varied during peak charging periods and other periods. Moreover, the commercial charging stations will charge additional service fees in addition to the basic charging price. The total charging fee for each PHEV varies according to the electric energy required to charge and the charging unit price.

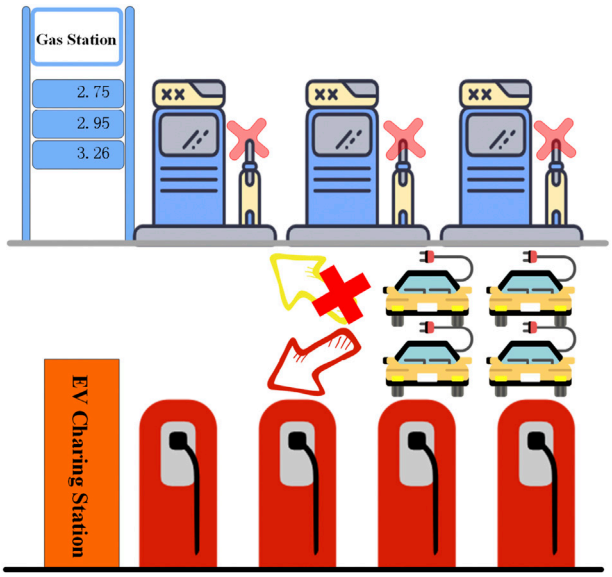

FIGURE 2 | Schematic diagram of PHEV energy acquisition with GSNs being attacked.

Next, considering the distance between the charging stations and the queue length of each charging station at the time instant t, the comprehensive index of each charging station can be calculated as follows:

$$Index = \alpha \times Q^i + \beta \times d_{s-s} + \gamma \times t^i_{wait} \tag{2}$$

where α, β, γ are the weight coefficients, d_{s-s} is the distance between the charging stations, and t^i_{wait} is the waiting time of the i^{th} PHEV. α, β, γ are decided by PHEV users. For example, some users pay more attention to fees, so the weight of the charging fees is relatively large.

Comparing the indicators of each charging station, the optimal charging station is selected as follows:

$$best = \min(Index\_A, Index\_B, Index\_C \ldots\ldots), \tag{3}$$

where $Index\_A$, $Index\_B$, $Index\_C$ are the comprehensive index of charging stations A, B, and C, respectively, calculated using **Eq. 2**.

The optimal charging station for the i^{th} PHEV at the time instant t is obtained using **Eqs 2**, **3**. PHEV users are encouraged to choose the optimal charging station to reduce the waiting time and charging cost. If the current charging station is the optimal charging station, the PHEV waits in place; otherwise, the i^{th} PHEV moves to the optimal charging station.

2.2 Mobile Charging Model of Plug-In Hybrid Electric Vehicles Under GSNs Attacked

According to the mobile charging strategy proposed above, the mobile charging model of PHEVs is established. In the PHEV

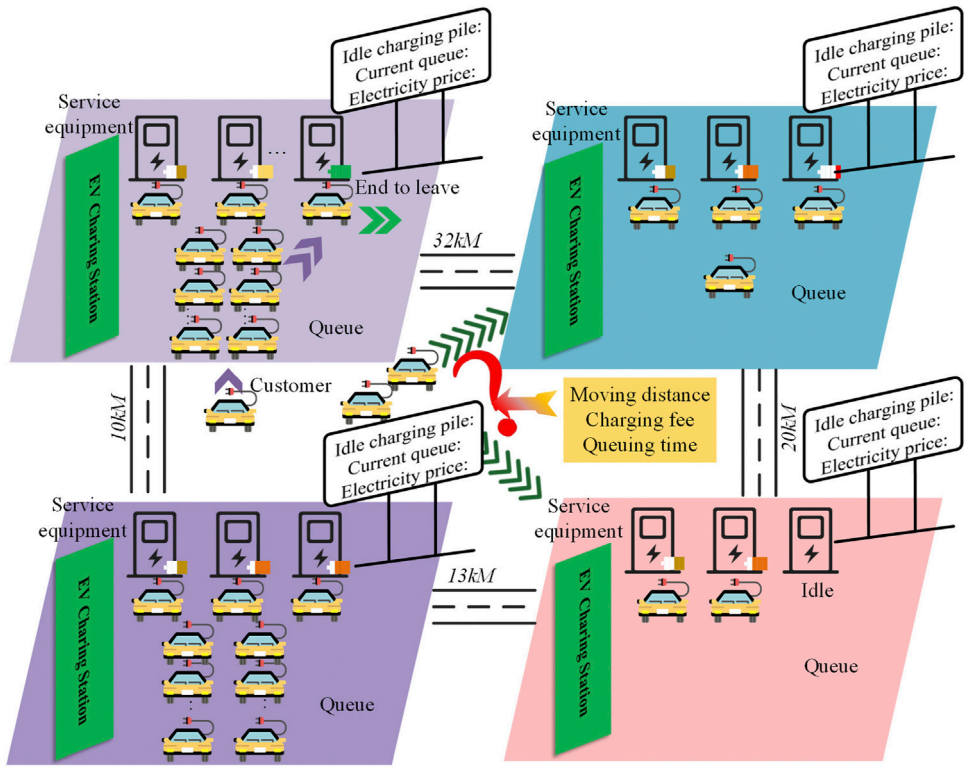

FIGURE 3 | Schematic diagram of the PHEV mobile charging strategy.

charging model with GSNs that have been attacked in the study by Li et al. (2020), the mismatch between the quantity of charging piles and PHEVs is ignored. There may be no idle charging piles when a PHEV arrives, especially during peak periods, as shown in **Figure 4**. Therefore, it is profitable for PHEV users to carry out the mobile charging.

To establish a PHEV charging model under GSNs that have been attacked, the daily commuting distance of PHEVs is analyzed. Through the statistical data analysis, the probability characteristic of the daily commuting distance of the vehicle conforms to the lognormal distribution (Li and Zhang (2012); Villanueva et al. (2011)). The probability density function (PDF) of the daily commuting distance for the i^{th} PHEV is expressed as follows:

$$f(x^i) = \frac{1}{x^i \sigma_D \sqrt{2\pi}} e^{-\frac{(\ln x^i - \mu_D)^2}{2\sigma_D^2}}, \tag{4}$$

where x^i is the daily commuting distance of the i^th PHEV, and μ_X and σ_X represent the mean and the variance of the lognormal distribution, respectively.

According to the driving distance in the combustion mode, the fuel consumption of the day can be obtained as follows:

$$gas_d^i = x_{gn}^i \times gas_p^i = (1 - OS^i)x^i \times gas_p^i, \tag{5}$$

where gas_p^i is the fuel consumption per kilometer of the i^{th} PHEV, OS^i is the OS of the i^{th} PHEV, and x_{gn}^i is the driving distance in the combustion mode.

When GSNs are unavailable, the driving distance in the combustion mode can be calculated using the following:

$$x_g^i = \begin{cases} (1 - OS^i)x^i, (1 - OS^i)x^i \times gas_p^i < gas_r^i \\ gas_r^i / gas_p^i, (1 - OS^i)x^i \times gas_p^i \geq gas_r^i \end{cases}, \tag{6}$$

where gas_r^i is the remaining fuel in the fuel tank of the i^{th} PHEV, which is assumed to obey a uniform distribution. It is worth noting that if the amount of remaining fuel can satisfy the commuting needs of the day, the distance traveled in the combustion mode is determined by the daily travel distance and the OS; otherwise, the distance traveled in the combustion mode depends on the amount of remaining fuel.

The driving distance in the electric mode x_e^i can be calculated from the daily travel distance x^i and the driving distance in the combustion mode x_g^i as follows:

$$x_e^i = x^i - x_g^i = \begin{cases} OS^i \times x^i, (1 - OS^i)x^i \times gas_p^i < gas_r^i \\ x^i - gas_r^i / gas_p^i, (1 - OS^i)x^i \times gas_p^i \geq gas_r^i \end{cases}. \tag{7}$$

Similarly, the driving distance in the electric mode is determined by the remaining fuel.

According to x_e^i, the state of charge (SOC) of the i^{th} PHEV at the end of the last trip to be charged can be derived as follows:

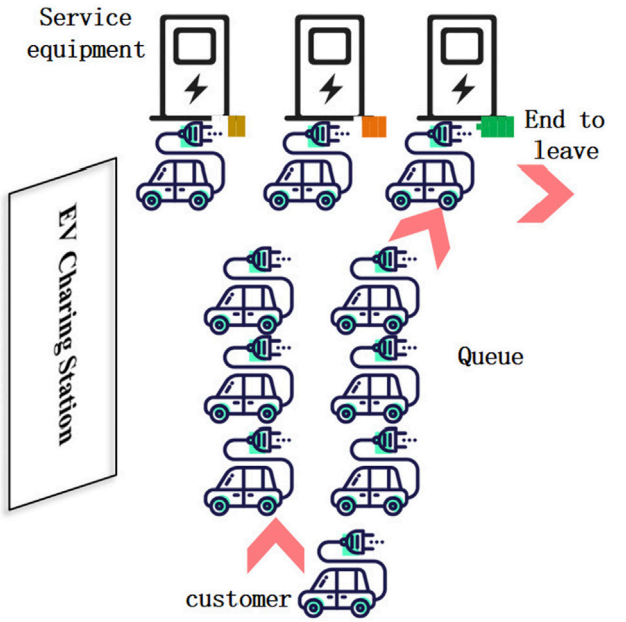

FIGURE 4 | PHEV queuing diagram.

$$SOC_0^i = \begin{cases} 1 - \dfrac{x_e^i \times e_t^i}{C^i} = 1 - \dfrac{x_e^i}{AER^i}, x_e^i < AER^i \\ 0, x_e^i \geq AER^i \end{cases}, \tag{8}$$

where e_t^i is the electric energy consumed by the PHEV per kilometer and the unit is *kWh/km*, C^i is the battery capacity and the unit is *kWh*, and AER^i represents the maximum distance that can be traveled in the electric mode when the battery is fully charged.

The power required to fully charge the i^{th} PHEV, E^i, can be obtained as follows:

$$E^i = \left(1 - SOC_0^i\right) \times C^i. \tag{9}$$

Then the charging duration of the i^{th} PHEV can be derived as follows:

$$T_c^i = \frac{E^i}{P_c^i \kappa^i}, \tag{10}$$

where P_c^i is the charging power, and κ^i is the charging efficiency.

For the convenience of modeling, it is assumed that the end of the last trip for PHEVs is the beginning of charging and that PHEVs are only charged once a day (Tian et al. (2010); Clement-Nyns et al. (2010)). As stated by statistics, the time of the start of charging conforms to the normal distribution, and its PDF can be expressed as follows:

$$f\left(t_s^i\right) = \begin{cases} \dfrac{1}{\sigma_{t_s}\sqrt{2\pi}} e^{-\frac{\left(t_s^i - \mu_{t_s}\right)^2}{2\sigma_{t_s}^2}}, \left(\mu_{t_s} - 12\right) < t_s^i \leq 24 \\ \dfrac{1}{\sigma_{t_s}\sqrt{2\pi}} e^{-\frac{\left(t_s^i + 24 - \mu_{t_s}\right)^2}{2\sigma_{t_s}^2}}, 0 < t_s^i \leq \left(\mu_{t_s} - 12\right) \end{cases}, \tag{11}$$

where t_s^i is the time instant of the start of charging for the i^{th} PHEV; $\mu_{t,s}$ and $\sigma_{t,s}$ represent the mean value and standard deviation of the starting time of charging, respectively. The time for each PHEV to reach the charging station is independent.

According to the first come first service (FCFS) queuing principle, the charging priority is set depending on the arrival time of PHEVs. To determine whether the PHEV arriving at time instant t can be charged immediately, it is necessary to know the working status of the charging pile at time instant t. The working status of the charging pile at time instant t can be expressed as follows:

$$State = \begin{cases} 0, 0 \leq N(t) < N_{charging} \\ 1, N(t) \geq N_{charging} \end{cases}, \tag{12}$$

where $N(t)$ is the number of PHEVs in the charging station at time instant t, and $N_{charging}$ denotes the amount of charging piles. The *State* value of 0 indicates that there are charging piles in the idle state; the *State* value of one indicates that all charging piles are in the working state.

Then, the remaining working time of all charging piles is sorted in ascending order at each moment. When the *State* value at time instant t is 1, the queue duration of the i^{th} PHEV, t_{wait}^i, is determined by the remaining working time of the charging piles and the required charging duration of PHEVs waiting in the queue. If there are charging piles in an idle status, the PHEV that arrives first will be arranged for charging; otherwise, it will continue to wait until a fully charged PHEV leaves.

According to the mobile charging strategy, if the current charging station is the optimal charging station, the ending time of charging is $t_s^i + T_c^i + t_{wait}^i$. When the ending time of charging $t_s^i + T_c^i + t_{wait}^i$ is less than 24, the charging load is given by the following:

$$P_w^i = \begin{cases} P_c^i, t_s^i + t_{wait}^i \leq t \leq t_s^i + T_c^i + t_{wait}^i \\ 0, 1 \leq t < t_s^i + t_{wait}^i, t_s^i + T_c^i + t_{wait}^i < t \leq T \end{cases}, \tag{13}$$

otherwise, the charging load is as follows:

$$P_w^i = \begin{cases} P_c^i, t_s^i + t_{wait}^i \leq t \leq T \\ 0, 1 \leq t < t_s^i + t_{wait}^i \end{cases}. \tag{14}$$

If the current charging station is not the optimal charging station, the moving time is calculated as follows:

$$t_{move}^i = \frac{d_{s-s}}{v^i}, \tag{15}$$

where v^i is the moving speed of the i^{th} PHEV. In this study, all PHEVs are assumed to drive at a constant speed.

Then the arrival time of the target charging station is as follows:

$$t_{arrive}^i = t + t_{move}^i \tag{16}$$

However, considering the remaining power of the PHEV including the remaining fuel and remaining power, the maximum travelable distance is obtained as follows:

$$d_{\max}^i = \max\left(\frac{gas_r^i}{gas_p^i}, \frac{SOC_0^i \times C^i}{e_{Traction}^i}\right). \tag{17}$$

When $d^i_{\max} > d_{s-s}$, it is possible for the PHEV to move to the selected target station. Conversely, the next best charging station is selected, that is, the optimal charging station is selected within the allowable range of the maximum driving distance.

The i^{th} PHEV may also be required to queue in the arrival station. There will be a new waiting time $t^i_{wait,2}$ calculated using the remaining working time of the charging piles and the required charging duration of PHEVs waiting in the queue in the arrival station. For the convenience of modeling, the consumption of electric power is neglected, that is, the charging duration T^i_c remains the same.

When the ending time of charging $t^i_{arrive} + t^i_{wait,2} + T^i_c$ is less than 24, the charging load in the optimal charging station is given as follows:

$$P^i_w = \begin{cases} P^i_c, t^i_{arrive} + t^i_{wait,2} \le t \le t^i_{arrive} + t^i_{wait,2} + T^i_c \\ 0, 1 \le t < t^i_{arrive} + t^i_{wait,2}, t^i_{arrive} + t^i_{wait,2} + T^i_c < t \le T \end{cases}, \quad (18)$$

otherwise, the charging load is as follows:

$$P^i_w = \begin{cases} P^i_c, t^i_{arrive} + t^i_{wait,2} \le t \le T \\ 0, 1 \le t < t^i_{arrive} + t^i_{wait,2} \end{cases}. \quad (19)$$

Then, the total charging load of all PHEVs in a single charging station is as follows:

$$P_{station\_k} = \sum_{i=1}^{N_{total}} P^k_{station\_t}, \quad (20)$$

where N_{total} is the total number of vehicles charged in a period.

3 RISK INDEX OF VOLTAGE VIOLATION BASED ON PROBABILISTIC LOAD FLOW

Probabilistic load flow (PLF) was proposed by Borkoaka in 1974 to solve the uncertainty in the power system and reflect the influence of random changes of various factors on the operation of the system. Considering the randomness of the distributed power generation and the PHEV load probability model in the grid, the PLF algorithm based on the 2m + 1 point estimation method (PEM) is employed to solve the voltage, and the risk of voltage violation is analyzed.

3.1 Correlation Transformation

To deal with the correlation of the input variables of PLF (wind speed, light intensity, daily load, *etc.*), Nataf transformation and elementary transformation (ET) are applied to transform the input variables in the correlated non-normal random vector space (CNNRVS) into the independent standard normal random vector space (ISNRVS) for the PEM (Li et al. (2020)). Wind speed, light intensity, and daily load variables can be described by Weibull distribution, Beta distribution, and normal distribution, respectively (Bilir et al. (2015); Cao et al. (2018); Ran and Miao (2016)). The PHEV charging load adopts the mobile charging model established above.

3.1.1 Nataf Transformation

Nataf transformation is used to transform the variables in the CNNRVS into the correlated standard normal random vector space (CSNRVS). It should be noted that Nataf transformation is applicable for variables known by the marginal distribution function and the correlation coefficient matrix. Specific steps are as follows.

As for input vector X, it is assumed that the cumulative distribution function (CDF) of the input variable $x_i\,(i = 1, 2, \cdots, n)$ is known. A random vector Z in the correlated standard normal space is introduced. The CDF is obtained as follows:

$$\begin{cases} \Phi(z_i) = F(x_i), \\ z_i = \Phi^{-1}[F(x_i)], \end{cases} \quad i = 1, 2, \ldots, m \quad (21)$$

where $\Phi(\cdot)$ and $\Phi^{-1}(\cdot)$ are the CDF and the inverse CDF of standard normal variables, respectively.

3.1.2 Elementary Transformation

After the Nataf transformation, the random vector Z in the CSNRVS is obtained, which needs to be transformed into the ISNRVS by ET transformation. ET transformation requires the use of two lemmas:

Lemma 1 (Knapp (2007)) It is assumed that R_Z is an n-dimensional non-negative real symmetric matrix. There is always an n-dimensional invertible matrix Q so that R_Z can be converted to a diagonal matrix R^*_Z using the following formula:

$$Q^T R_Z Q = R^*_Z. \quad (22)$$

Lemma 2 (Bauer (1996)) If there is an n-dimensional invertible matrix that conforms to **Eq. 23**, then **Eq. 24** is also satisfied, as follows:

$$(Y_1, Y_2, \cdots, Y_n) = (Z_1, Z_2, \cdots, Z_n)diag\left(\sigma^{-1}_{Z_1}, \sigma^{-1}_{Z_2}, \cdots, \sigma^{-1}_{Z_n}\right)Q, \quad (23)$$

$$COV(Y) = \left(diag\left(\sigma^{-1}_{Z_1}, \sigma^{-1}_{Z_2}, \cdots, \sigma^{-1}_{Z_n}\right)Q\right)^T COV(Z)\left(diag\left(\sigma^{-1}_{Z_1}, \sigma^{-1}_{Z_2}, \cdots, \sigma^{-1}_{Z_n}\right)Q\right), \quad (24)$$

where $COV(Z)$ is the covariance of Z, $COV(Y)$ is the covariance of Y, and σ_{Z_i} is the standard deviation of z_i.

The correlation coefficient matrix of the correlated standard normal random vector R_Z satisfies the following formula:

$$R_Z = \left(diag\left(\sigma^{-1}_{Z_1}, \sigma^{-1}_{Z_2}, \cdots, \sigma^{-1}_{Z_n}\right)\right)^T COV(Z) diag\left(\sigma^{-1}_{Z_1}, \sigma^{-1}_{Z_2}, \cdots, \sigma^{-1}_{Z_n}\right). \quad (25)$$

The vector Z obeys the normal distribution, and the components have correlation.According to the definition of the covariance matrix, it can be known that $COV(Z)$ is a non-negative real symmetric matrix and $diag(\sigma^{-1}_{Z_1}, \sigma^{-1}_{Z_2}, \cdots, \sigma^{-1}_{Z_n})$ is an invertible matrix. It can be seen that R_Z is a non-negative real symmetric matrix (31 (????)).

According to Lemma 1, combining **Eq. 25**, the following result is obtained:

$$\left(diag\left(\sigma^{-1}_{Z_1}, \sigma^{-1}_{Z_2}, \cdots, \sigma^{-1}_{Z_n}\right)Q\right)^T COV(Z)\left(diag\left(\sigma^{-1}_{Z_1}, \sigma^{-1}_{Z_2}, \cdots, \sigma^{-1}_{Z_n}\right)Q\right) = R^*_Z. \quad (26)$$

According to Lemma 2, the random vector Y can be obtained. Comparing **Eq. 24** with **Eq. 26**, it can be seen that $COV(Y)$ is a

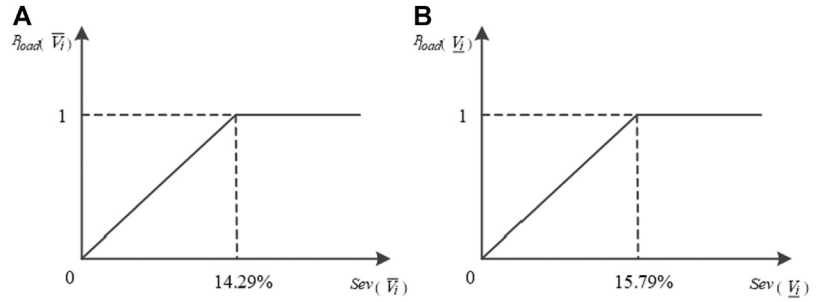

FIGURE 5 | Load loss when voltages exceed the security limits. **(A)** Voltage exceeds the upper limit. **(B)** Voltage exceeds the lower limit.

diagonal matrix, and Y_i and Y_j are linearly independent. Z in the CSNRVS is transformed into Y in the ISNRVS.

3.2 Probabilistic Load Flow Based on 2m + 1 PEM

The Monte Carlo and PE methods are commonly used to solve PLF. Although the Monte Carlo method is highly accurate, it is computationally intensive. Compared with the Monte Carlo method, the PEM can not only reduce computational burden but also achieve high accuracy by using the generated input variable samples, which becomes a good alternative to the Monte Carlo method. There are several different PEM approaches; the 2m + 1 PEM is widely used in PLF because it involves less calculation and higher accuracy than other PE methods (Che et al. (2020); Xia et al. (2016)). The 2m + 1 PEM is also called the 3m method. For m input variables, 3m estimated points are constructed while m points correspond to the same estimated point vector, so the 3m PEM is transformed to the 2m + 1 PEM. The specific method is as follows.

The estimated value y_i of the i^{th} input variable Y_i can be obtained as follows:

$$y_{i,k} = \mu_{y_i} + \xi_{i,k}\sigma_{y_i}, k = 1, 2, 3, \tag{27}$$

where μ_{y_i} and σ_{y_i} are the mean and deviation of Y_i. $\xi_{i,k}$ is the position measurement coefficient of the estimated value, as shown below:

$$\begin{cases} \xi_{i,k} = \dfrac{\nu_{y_i}}{2} + (-1)^{3-k}\sqrt{\lambda_{y_i} - \dfrac{3}{4}\nu_{y_i}^2}, k = 1, 2 \\ \xi_{i,3} = 0 \end{cases}, \tag{28}$$

where ν_{y_i} and λ_{y_i} are the skewness coefficient and the kurtosis coefficient of y_i. $\xi_{i,3} = 0$ indicates that $y_{i,3}$ is the mean value of y_i.

When other input variables take the mean value, the variable y_i is replaced by each estimate $y_{i,k}$ in turn. The original sample matrix $Y \in \mathfrak{R}^{n\times m}$ is reduced to an estimated point matrix $Y' \in \mathfrak{R}^{(2m+1)\times m}$. After the construction of the estimates is completed, the estimated point matrix $Y' \in \mathfrak{R}^{(2m+1)\times m}$ is transformed from the ISNRVS to the original space $X' \in \mathfrak{R}^{(2m+1)\times m}$ by inverse ET and inverse Nataf transformation.

According to the analysis above, the input vector $X' \in \mathfrak{R}^{(2m+1)\times m}$ is obtained, including the charging load of PHEVs, daily load, wind speed, light intensity, and other information. Then the deterministic load flow is operated 2m + 1 times. To the end, the output vector $W = (W_1, W_2, \cdots W_{2m+1})$ composed of branch power flows and nodal voltages is obtained. The l^{th} moment W can be expressed as follows:

$$E\left(W^l\right) \approx \sum_{i=1}^{m}\left[\omega_{i,1}\left(W_{2i-1}\right)^l + \omega_{i,2}\left(W_{2i}\right)^l\right] + \omega_{2m+1}\left(W_{2m+1}\right)^l, \tag{29}$$

where E represents the mean operator, and $\omega_{i,j}$ is the probability concentration. The mean and standard deviation of the output variable can be expressed as follows:

$$\mu_W = E(W), \tag{30}$$

$$\sigma_W = \sqrt{E(W^2) - [E(W)]^2}. \tag{31}$$

The specific procedures of PLF are designated in **Algorithm 1**:

Algorithm 1: Procedures of PLF

Input: X_w, X_{pvg}, X_L, X_{PHEV}
Output: Vol
(Z_w, Z_{pvg}) = Nataf (X_w, X_{pvg})
$(Y_w, Y_{pvg}, Y_L, Y_{PHEV})$ = ET$(Z_w, Z_{pvg}, X_L, X_{PHEV})$
$Y \leftarrow [Y_w, Y_{pvg}, Y_L, Y_{PHEV}]$
for i = 1:m
  $\nu_{y,i}$ = Skewness (Y_i)
  $\lambda_{y,i}$ = Kurosis (Y_i)
  Calculate $\xi_{i,k}$ according to (28)
  $\mu_{y,i}$ = Mean (Y_i)
  $\sigma_{y,i}$ = Var (Y_i)
  for k = 1:3
    $y_{i,k} = \mu_{y_i} + \xi_{i,k}\sigma_{y_i}$
  end
  $(Y'_w, Y'_{pvg}, Y'_L, Y'_{PHEV})$ = Ponit $(y_{i,k})$
end
$(X'_w, X'_{pvg}, X'_L, X'_{PHEV})$ = Inverse $(Y'_w, Y'_{pvg}, Y'_L, Y'_{PHEV})$
(P_w, P_{pvg}) = Generation (X'_w, X'_{pvg})
for i = 1:2m + 1
  v = Flow $(P_w, P_{pvg}, X'_L, X'_{PHEV})$
  $Vol = Vol + \xi v$
end

Input and Output: X_w, X_{pvg}, X_L, and X_{PHEV} are wind speeds, light intensity, basic load, and charging load of the PHEV. Vol is the voltage of the power grid.

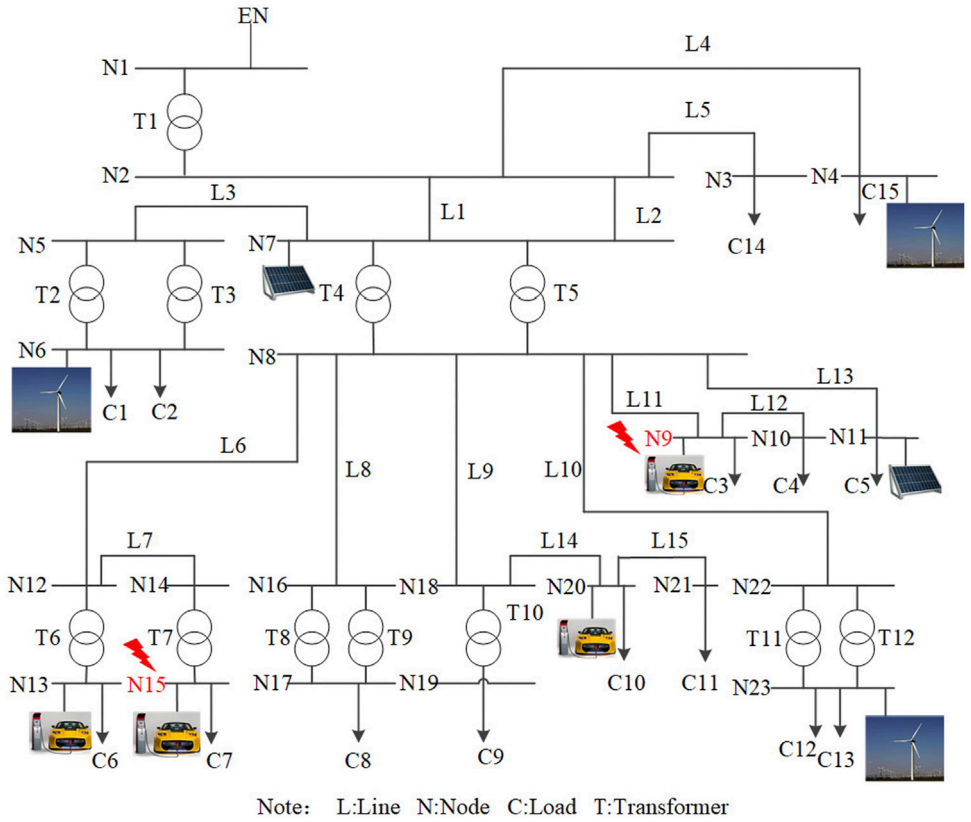

FIGURE 6 | Modified real coastal active distribution network.

3.3 Risk Index of Voltage Violation

The voltage violation risk of the i^{th} node in the k period is calculated using the voltage violation probability $P(V_i^k)$ and the corresponding load loss $P_{load}(V_i^k)$ as follows:

$$R\left(V_i^k\right) = P\left(V_i^k\right)P_{load}\left(V_i^k\right), \tag{32}$$

where V_i^t is the voltage of the i^{th} node in the k period.

The probability of voltage violation can be obtained from the voltage distribution of PLF results. In general, the voltage distribution obeys normal distribution. The probability of voltage violation can be expressed as follows:

$$P\left(V_i^k\right) = F_I\left(V_i^k \notin \left[V_{imin}^k, V_{i\max}^k\right]\right), I = \left|V_i^k - \mu_{V_i^k}\right| < 3\sigma_{V_i^k}, \tag{33}$$

where $V_{i\max}^k$ and V_{imin}^k indicate the upper and lower limits of the node voltage and are set as 1.05 and 0.95 of the rated voltage, respectively. $\mu_{V_i^k}$ and $\sigma_{V_i^k}$ are the mean and standard deviation of the nodal voltage. I is the confidence level when the sample data of the voltage follow the "3σ principle." F is the CDF of V_i^k. The probability of voltage violation includes the probability of exceeding the upper limit and exceeding the lower limit.

The severity of the voltage violation is presented as follows:

$$\mathrm{Sev}\left(V_i^k\right) = \begin{cases} \mathrm{Sev}\left(\overline{V}_i^k\right) = \left|\dfrac{V_i^k - V_{i\max}^k}{V_{i\max}^k}\right|, V_i^k > V_{i\max}^k \\ \mathrm{Sev}\left(\underline{V}_i^k\right) = \left|\dfrac{V_i^k - V_{i\min}^k}{V_{i\max}^k}\right|, V_i^k < V_{i\max}^k \end{cases} \tag{34}$$

where $\mathrm{Sev}(\overline{V}_i^k)$ and $\mathrm{Sev}(\underline{V}_i^k)$ indicate the severity index when the node voltage exceeds the upper limit and the lower limit, respectively.

The corresponding load loss can be derived using the severity of the voltage violation. The relationship between severity and load loss is linear within a certain range, as shown in **Figure 5**. The critical value of the upper severity is 14.29% ($|(1.2 - 1.05)/1.05|$). The critical value of the lower severity is 15.79% ($|(0.8 - 0.95)/0.95|$). The action threshold of overvoltage protection is set as 1.2 times the rated voltage value. The threshold of overvoltage is set as 1.05 times the rated voltage value. The critical value of the lower severity is the same.

The charging load increases after GSNs are attacked, and it is an indisputable fact that the voltage level decreases and the risk of voltage violation increases. PHEVs in the attacked area are motivated to perform mobile charging using the proposed mobile charging strategy. The charging stress in the

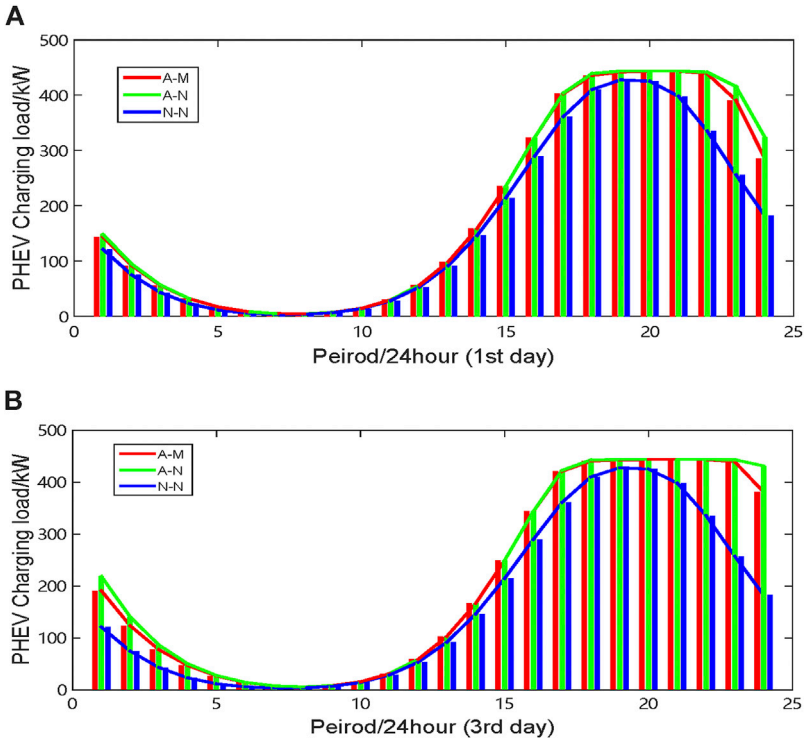

FIGURE 7 | Load variation of charging station A. **(A)** Charging load in the first 24 h (1st day). **(B)** Charging load in the third 24 h (3rd day) (A–M, GSNs are attacked and PHEVs move to charge; A–N, GSNs are attacked and PHEVs do not move to charge; N–N, GSNs work normally and PHEVs do not move to charge).

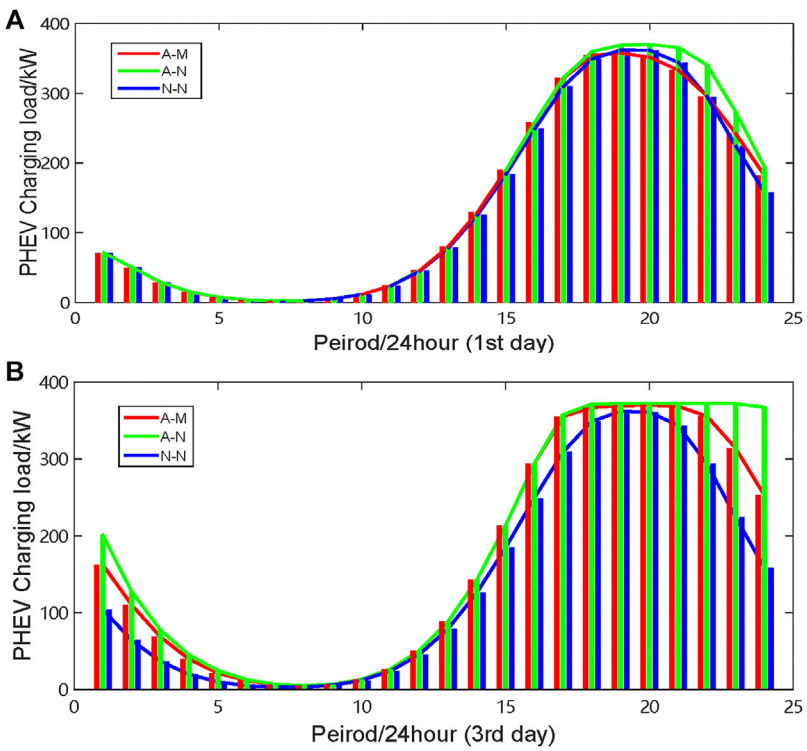

FIGURE 8 | Load variation of charging station C. **(A)** Charging load in the first 24 h (1st day). **(B)** Charging load in the third 24 h (3rd day).

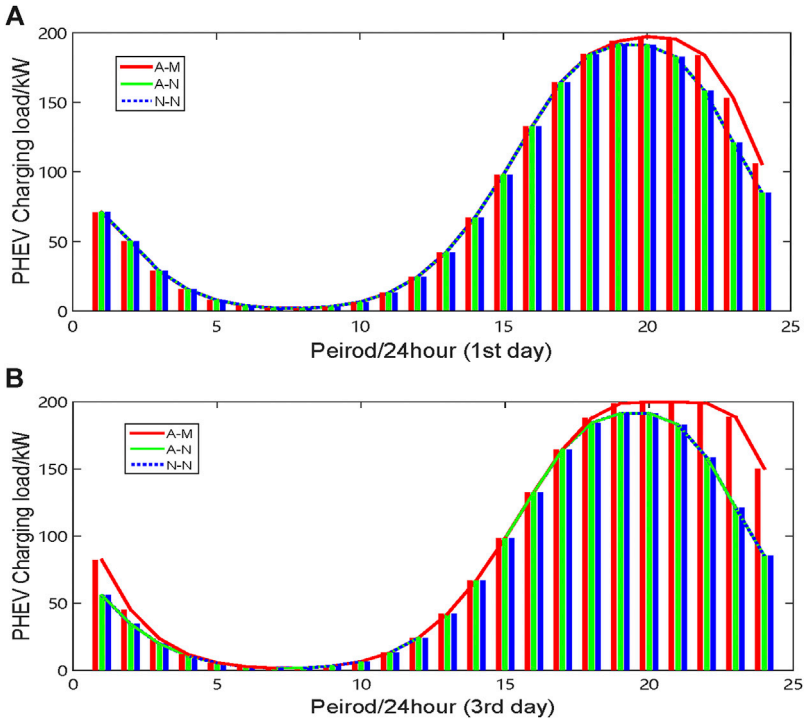

FIGURE 9 | Load variation of charging station B. **(A)** Charging load in the first 24 h (1st day). **(B)** Charging load in the third 24 h (3rd day).

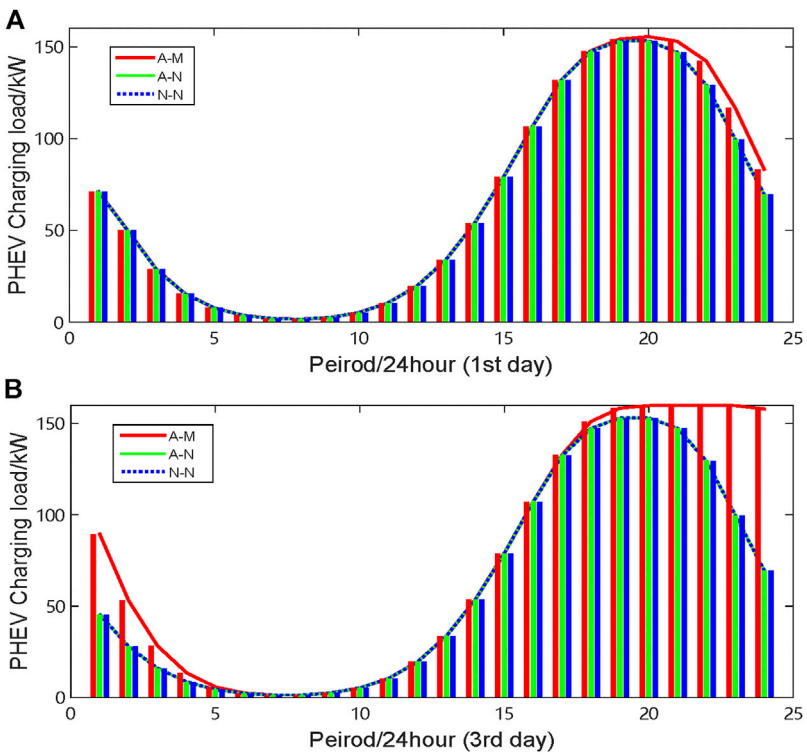

FIGURE 10 | Load variation of charging station D. **(A)** Charging load in the first 24 h (1st day). **(B)** Charging load in the third 24 h (3rd day).

TABLE 1 | Comparison of the waiting time before and after mobile charging.

Case	Waiting time (min)									
Before mobile charging	47	38	23	30	30	29	35	24	34	76
After mobile charging	17	5	0	0	1	0	4	3	0	30

attacked area is then abated, which reduces the risk of voltage violation.

4 SIMULATIONS

The modified coastal active power distribution network is used as a case study to analyze the impact of the proposed mobile charging strategy on the voltage (Strugar et al. (2013)), as shown in **Figure 6**. Three wind farms and two photovoltaic systems are installed at nodes 3, 4, 6, 11, and 17, respectively. Four charging stations (A, B, C, and D) are considered in nodes 9, 13, 15, and 20. It is assumed that there are 14,000 residents in the area and the quantities of vehicles per capita is 291 vehicles per 1,000 people (RS.Statistical Office (2016)). Moreover, the penetration rate of PHEVs is set as 35%; it indicates that the network has about 1,426 PHEVs (Li et al. (2020)). It is being supposed that gas stations in the area located in nodes 9 and 15 cannot provide gas service due to GSNs being attacked, and only the charging stations work normally. In other words, GSNs in the area containing the charging stations A and C are attacked, while GSNs in the areas containing the charging stations B and D work normally. In this part, the effectiveness of the proposed strategy is verified by comparing these three situations: GSNs are attacked and PHEVs move to charge (A–M), GSNs are attacked and PHEVs do not move to charge (A–N), and GSNs work normally and PHEVs do not move to charge (N–N).

4.1 The Impact of Mobile Charging Strategy on Charging Load

In general, there is not a lot of surplus of charging piles, especially when GSNs are unavailable. This phenomenon adds congestion to the charging station, as shown in **Figures 7**, **8**. It is obvious that the charging loads at charging stations A and C increase due to the unavailability of GSNs. Moreover, the charging stations A and C are fully loaded for a long time during peak charging periods. In other words, PHEVs arriving at the peak charging period will have to queue for a long time.

Moreover, the fully loaded duration of the charging station is prolonged by an increase during the attacked time, as depicted in **Figures 7B**, **8B**. As can be observed, the charging load in case of A-N almost remains the highest during 17:00–24:00, which means that the more severe charging congestion occurs in the charging station. The charging jams and greater dependence of PHEVs on electric energy proves that mobile charging is essential.

According to this mobile charging strategy, a portion of PHEV users who originally charged at charging stations A and C are encouraged to move to stations B and D for charging. Hence, the comprehensive economic and time benefits of users are protected. Consequently, the charging stress of charging stations A and C is dispersed, and the fully loaded duration of charging stations A and C decreases, as shown by the red curves in **Figures 7**, **8**. It is noteworthy that all charging piles are involved, to work in stations A and C during 17:00–21:00 in case of 72 h of attack. In this case, it does not illustrate that mobile charging has not occurred. As long as there are PHEVs in the queue, the charging stations are still fully loaded. Overall, the congestion in stations A and C is suitably improved.

Figures 9, **10** present the load variations of stations B and D. It is clear that the charging loads of charging stations B and D increase during the peak charging periods *via* mobile charging of PHEVs. Additionally, the longer the GSNs are attacked, the greater the number of PHEVs going to charging stations B and D. As a result, the charging congestion occurs in stations B and D. The worst case is presented in **Figure 8B**. In fact, although there is a queue at station D, it is still the optimal choice for some PHEV users. According to **Figures 7**–**10**, it is obvious that the mobile charging strategy is effective for relieving the charging stress in attacked areas.

Each PHEV has its own waiting time and charging fee, so there are 1,426 cases in this simulation. Here, 10 distinct results of the waiting time and charging fee before and after mobile charging are presented in **Tables 1**, **2**. It can be seen from **Table 1** that after PHEVs move to the optimal charging station, the waiting time of four PHEVs is zero, while the waiting time of

TABLE 2 | Comparison of the charging fee before and after mobile charging.

Case	Charging fee (RMB)									
Before mobile charging	12	16.25	26.75	47.75	24.25	24.5	22.5	38	40.75	35.75
After mobile charging	14.4	19.5	32.1	54.9	29.1	29.4	27	18.5	48.9	42.9

TABLE 3 | Comparison of the comprehensive index before and after mobile charging.

Case	Comprehensive index									
Before mobile charging	22.4	20.08	26.75	27.75	24.25	21.35	22.5	28	20.75	15.75
After mobile charging	20.62	18.35	22.35	24.9	19.1	18.92	18.36	22.5	18.9	12.9

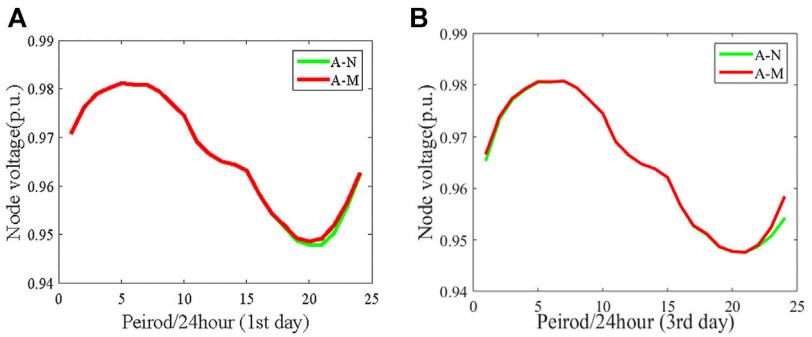

FIGURE 11 | Voltage comparison of node 15 for different attack durations. **(A)** First 24 h (1st day). **(B)** Third 24 h (3rd day).

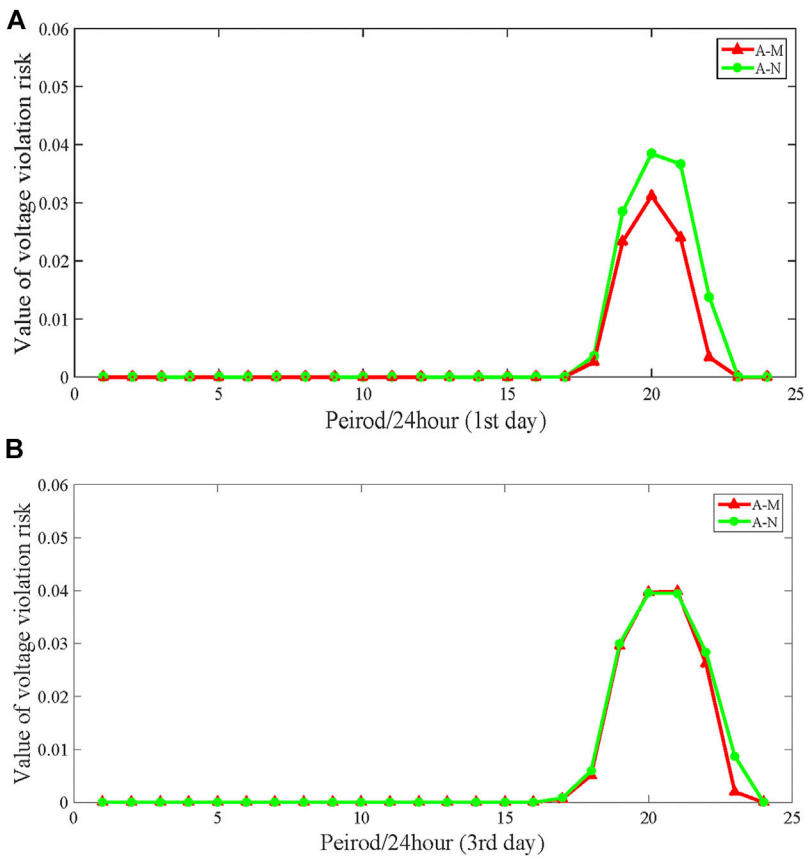

FIGURE 12 | Comparison of the voltage violation risk of node 15 for different attack durations. **(A)** First 24 h (1st day). **(B)** Third 24 h (3rd day).

six PHEVs decreases significantly. Meanwhile, it is found from **Table 2** that the charging fee of one PHEV decreases significantly, while the charging fee of nine PHEVs increases slightly after mobile charging. It is seen from **Table 3** that although the charging fee increases, the waiting time is shortened, and the comprehensive index is better. Therefore, PHEVs choose mobile charging instead of waiting in place. When the current charging station is optimal, PHEVs will wait in place for charging, so the charging cost and waiting time will not change.

4.2 The Impact of Mobile Charging Strategy on the Voltage Violation Risk

For further analysis, the risk of voltage violation is presented to illustrate the effect of the mobile charging strategy.

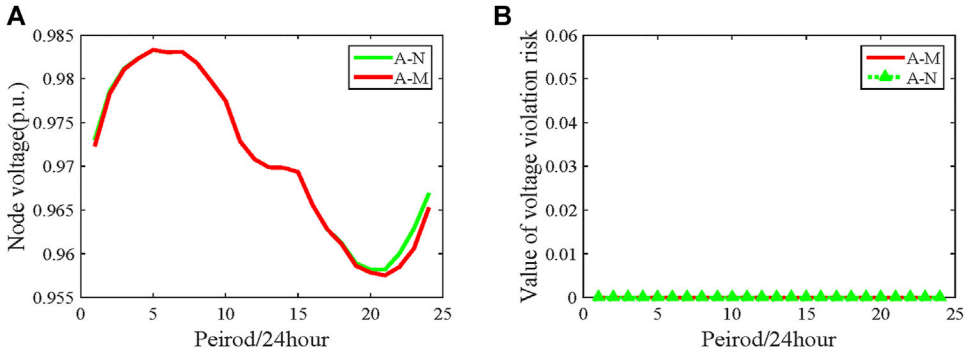

FIGURE 13 | Voltage analysis of node 13. **(A)** Voltage comparison of node 13 in the first 24 h (1st day). **(B)** Comparison of risk in the third 24 h (3rd day).

Considering the similarity of the load variation shown above, only node 13 (connected by the charging station) and node 15 (connected by charging station C) are taken as the examples to analyze.

Figure 11 depicts the voltage comparison of node 15. A voltage drop can be observed when GSNs are unavailable. In addition, as the attack time is prolonged, the voltage drops more. However, due to the limitation of the charging piles, the voltage does not drop excessively. It is obvious that the duration that the voltage is at a lower level is longer due to the extension of the fully loaded periods. For the mobile charging strategy, the voltage of node 15 at peak periods rises up in the first 24 h of attack (first day). Consequently, the risk of voltage violation decreases significantly as shown in **Figure 12A**. In the case of the first 72 h of attack, no matter whether PHEVs move or not, station C is always fully loaded during 17:00–21:00, resulting in a little change in the voltage and the risk of voltage violation. After 21:00, the voltage increases and the risk of voltage violation decreases because of a decrease in the charging load of station C, as shown in **Figures 11B**, **12B**. In conclusion, the charging load of PHEVs is dispersed using the mobile charging strategy, and the voltage level increases and the risk of voltage violation is reduced.

Figure 13 shows the voltage and the violation risk of node 13. After mobile charging of PHEVs, it is obvious that the voltage during the peak charging period decreases because of the increase in the charging demand. However, the risk of voltage violation is always at 0, as shown in **Figure 13B**, denoting that the risk is not affected by mobile charging of PHEVs. In fact, although the voltage of node 13 drops on using the mobile charging strategy, it does not cause the voltage limit to be exceeded, that is, the increasing load is within its acceptable range.

5 CONCLUSION

For a surge of the PHEV charging load under the regional GSNs being attacked, this study investigates the risk of voltage violation after the mobile charging of PHEVs. In view of the phenomenon of charging congestion under GSNs that have been attacked, the mobile charging strategy is proposed to encourage users to charge movably. The charging fee, queueing time, and location of the charging station are emphasized, and the mobile charging model is developed to relieve the charging stress of charging stations in the attacked areas. Then the PLF based on the 2m + 1 PEM is used to obtain the voltage distribution, and a risk index of voltage violation is set up to analyze the impact of PHEV mobile charging.

The validation of the proposed mobile charging strategy is performed on the modified coastal active power distribution network. The results demonstrate that the charging load in the attacked area of GSNs is significantly reduced, which further indicates that PHEVs are encouraged to move using the mobile charging strategy, and the full-loaded time is sharply decreased. After mobile charging, the charging stress of charging stations located in the attacked area is dispersed and the voltage level rises. Therefore, it indicates that the risk of voltage violation can be reduced using the proposed mobile charging strategy. It is worth mentioning that the security constraint of charging stations located in unattacked areas is neglected. However, the excessive movement of PHEVs may lead to an increase in the risk of voltage violation in normal areas, although the risk in normal areas has always been zero in this work. Therefore, more security constraints can be investigated in future work.

DATA AVAILABILITY STATEMENT

The original contributions presented in the study are included in the article/Supplementary Material; further inquiries can be directed to the corresponding authors.

AUTHOR CONTRIBUTIONS

All authors listed have made a substantial, direct, and intellectual contribution to the work and approved it for publication.

FUNDING

This research was funded by the National Science Foundation of China (Grant nos. 61773253, 61803252, and 61633016), the Project of Science and Technology Commission of Shanghai Municipality, China (20JC1414000, 19500712300, and 19510750300) and Shanghai Talent development Foundation.

ACKNOWLEDGMENTS

This work was supported by the Shanghai Key Laboratory of Power Station Automation Technology, Shanghai University. The authors would like to thank reviewers for their careful work. Their most helpful and constructive comments improve the quality of the article.

REFERENCES

Badawy, M. O., and Sozer, Y. (2017). Power Flow Management of a Grid Tied Pv-Battery System for Electric Vehicles Charging. *IEEE Trans. Ind. Applicat.* 53, 1347–1357. doi:10.1109/TIA.2016.2633526

Bauer, H. (1996). Probability Theory *(Gerike Gmbh)*. Berlin, Germany.

Bilir, L., İmir, M., Devrim, Y., and Albostan, A. (2015). Seasonal and Yearly Wind Speed Distribution and Wind Power Density Analysis Based on Weibull Distribution Function. *Int. J. Hydrogen Energ.* 40, 15301–15310. doi:10.1016/j.ijhydene.2015.04.140

Cai, Z., Shu, H., Yang, B., and Shan, J. (2021). Research on Regional Dispatching Plan and Coordinated Charging Strategy of Electric Bus. *Power Syst. Technology* 1070-1072, 1632–1636. doi:10.13335/j.1000-3673.pst.2020.1922

Cao, Y., Zhang, Y., Zhang, H., Shi, X., and Terzija, V. (2018). Probabilistic Optimal Pv Capacity Planning for Wind Farm Expansion Based on Nasa Data. *IEEE Power Energ. Soc. Gen. Meet. (Pesgm)*. 8(3): 1. doi:10.1109/PESGM.2018.8585748

Che, Y., Wang, X., Lv, X., and Hu, Y. (2020). Probabilistic Load Flow Using Improved Three point Estimate Method. *Int. J. Electr. Power Energ. Syst.* 117, 105618. doi:10.1016/j.ijepes.2019.105618

Chen, L., and Huang, X. (2019). Ordered Charging Strategy of Electric Vehicles at Charging Station on Highway. *Electric Power Automation Equipment* 39, 112–117+126. doi:10.16081/j.issn.1006-6047.2019.01.017

Clement-Nyns, K., Haesen, E., and Driesen, J. (2010). The Impact of Charging Plug-In Hybrid Electric Vehicles on a Residential Distribution Grid. *IEEE Trans. Power Syst.* 25, 371–380. doi:10.1109/TPWRS.2009.2036481

Dong, Q., Niyato, D., Wang, P., and Han, Z. (2016). The Phev Charging Scheduling and Power Supply Optimization for Charging Stations. *IEEE Trans. Veh. Technol.* 65, 566–580. doi:10.1109/TVT.2015.2399411

Du, D., Chen, R., Li, X., Wu, L., Zhou, P., and Fei, M. (2019a). Malicious Data Deception Attacks against Power Systems: A New Case and its Detection Method. *Trans. Inst. Meas. Control.* 41, 1590–1599. doi:10.1177/0142331217740622

Du, D., Li, X., Li, W., Chen, R., Fei, M., and Wu, L. (2019b). Admm-based Distributed State Estimation of Smart Grid under Data Deception and Denial of Service Attacks. *IEEE Trans. Syst. Man. Cybern, Syst.* 49, 1698–1711. doi:10.1109/TSMC.2019.2896292

Fouladi, E., Baghaee, H. R., Bagheri, M., and Gharehpetian, G. B. (2019). A Charging Strategy for Phevs Based on Maximum Employment of Renewable Energy Resources in Microgrid. In 2019 IEEE International Conference on Environment and Electrical Engineering and 2019 IEEE Industrial and Commercial Power Systems Europe (EEEIC/I CPS Europe). Genova, Italy. 11-14 June 2019, IEEE. 1–5. doi:10.1109/EEEIC.2019.8783742

Chao, H., Li, J., and Peng, D. (2018). Model Predictive Control of Batch Processes Based on Two-Dimensional Integration Frame. *Nonlinear Anal. Hybrid Syst.* 28, 75–86. doi:10.1016/j.nahs.2017.11.002

Knapp, A. (2007). Advanced Algebra *(Birkhauser)*. Berlin, Germany: Springer.

Ko, H., Pack, S., and Leung, V. C. M. (2018). Mobility-aware Vehicle-To-Grid Control Algorithm in Microgrids. *IEEE Trans. Intell. Transport. Syst.* 19, 2165–2174. doi:10.1109/TITS.2018.2816935

Li, G., and Zhang, X.-P. (2012). Modeling of Plug-In Hybrid Electric Vehicle Charging Demand in Probabilistic Power Flow Calculations. *IEEE Trans. Smart Grid* 3, 492–499. doi:10.1109/TSG.2011.2172643

Li, X., Dong, J., Du, D., Wu, L., and Fei, M. (2020). Impact of Phev in Active Distribution Network under Gas Station Network Attack. *ISA Trans.* 104, 192–203. doi:10.1016/j.isatra.2019.02.024

Li, X., Jiang, C., Du, D., Wang, R., Fei, M., Li, X., et al. (2021). Optimization and Control of Cyber-Physical Power Systems under Dual-Network Interactive Cascading Failure. *Control. Eng. Pract.* 111, 104789. doi:10.1016/j.conengprac.2021.104789

Liu, A., Yuan, X., and Li, J. (2018a). Research on Orderly Charging Strategy of Electric Vehicle under Urban Distribution Network. *Electr. Meas. Instrumentation* 55, 55–55+74.

Liu, D., Zhong, Q., Zhong, Q., Wang, Y., and Liu, G. (2018b). Modeling and Control of a V2g Charging Station Based on Synchronverter Technology. *Csee Jpes* 4, 326–338. doi:10.17775/CSEEJPES.2016.01430

Maigha and Crow, M. (2014). Economic Scheduling of Residential Plug-In (Hybrid) Electric Vehicle (PHEV) Charging. *Energies* 7, 1876–1898. doi:10.3390/en7041876

Nafisi, H., Askarian Abyaneh, H., and Abedi, M. (2016a). Energy Loss Minimization Using Phevs as Distributed Active and Reactive Power Resources: a Convex Quadratic Local Optimal Solution. *Int. Trans. Electr. Energ. Syst.* 26 (6), 1287–1302. doi:10.1002/etep.2134

Nafisi, H., Agah, S. M. M., Askarian Abyaneh, H., and Abedi, M. (2016b). Two-stage Optimization Method for Energy Loss Minimization in Microgrid Based on Smart Power Management Scheme of Phevs. *IEEE Trans. Smart Grid* 7, 1268–1276. doi:10.1109/TSG.2015.2480999

Nornagoro, A., Banjar-Nahor, K. M., Rahman, F. S., Rahmani, R., and Hariyanto, N. (2020). Impact of Combined Electric Vehicle and Pv Parking Lot to Reliability of Distribution Network Systems and its Mitigations. In 2020 International Conference on Technology and Policy in Energy and Electric Power (ICT-PEP), Bandung, Indonesia, 23-24 Sept. 2020, IEEE, 283–288. doi:10.1109/ICT-PEP50916.2020.9249941

Pouladi, J., Bannae Sharifian, M. B., and Soleymani, S. (2016). Determining Charging Load of Phevs Considering Hvac System and Analyzing its Probabilistic Impacts on Residential Distribution Network. *Electric Power Syst. Res.* 141, 300–312. doi:10.1016/j.epsr.2016.08.008

Ran, X., and Miao, S. (2016). Three-phase Probabilistic Load Flow for Power System with Correlated Wind, Photovoltaic and Load. *IET Generation, Transm. Distribution* 10, 3093–3101. doi:10.1049/iet-gtd.2016.0424

RS.Statistical Office (2016). Statistical Yearbook *(Statistical Office of the Republic of Serbia)*.

Salehi, J., and Abdolahi, A. (2019). Optimal Scheduling of Active Distribution Networks with Penetration of Phev Considering Congestion and Air Pollution Using Dr Program. *Sustainable Cities Soc.* 51, 101709. doi:10.1016/j.scs.2019.101709

Strugar, L., Katic, V. A., and Milanovic, J. V. (2013). Generic Model of Coastal Distribution Network for Power System Harmonics Studies. *Przeglad Elektrotechniczny* 89, 149–155.

Tian, L., Shi, S., and Jia, Z. (2010). A Statistical Model for Charging Power Demand of Electric Vehicles. *Power Syst. Technology* 34, 126–130. doi:10.13335/j.1000-3673.pst.2010.11.020

Villanueva, D., Pazos, J. L., and Feijoo, A. (2011). Probabilistic Load Flow Including Wind Power Generation. *IEEE Trans. Power Syst.* 26, 1659–1667. doi:10.1109/TPWRS.2010.2096436

Wang, L., Liu, C., Wang, B., and Cai, L. (2018). Risk Based Assessment Method for Transmission System Considering the Influence of Micro-grid Charging Station. *Power Syst. Prot. Control.* 46, 114–121.

Xia, S., Luo, X., Chan, K. W., Zhou, M., and Li, G. (2016). Probabilistic Transient Stability Constrained Optimal Power Flow for Power Systems with Multiple Correlated Uncertain Wind Generations. *IEEE Trans. Sustain. Energ.* 7, 1133–1144. doi:10.1109/TSTE.2016.2520481

Xie, X., Yue, D., and Peng, C. (2018). Relaxed Real-Time Scheduling Stabilization of Discrete-Time Takagi-Sugeno Fuzzy Systems via an Alterable-Weights-Based Ranking Switching Mechanism. *IEEE Trans. Fuzzy Syst.* 26, 3808–3819. doi:10.1109/TFUZZ.2018.2849701

Yang, X., Yi, Y., Zhang, Y., Mo, Y., Huang, T., and Xie, X. (2020). Operation Risk Analysis of Electric Vehicle Integrated to Distribution Network Based on Weighted Distribution Entropy. *Automation Electric Power Syst.* 044, 171–179.

Zeng, M., Leng, S., Zhang, Y., and He, J. (2018). Qoe-aware Power Management in Vehicle-To-Grid Networks: A Matching-Theoretic Approach. *IEEE Trans. Smart Grid* 9, 2468–2477. doi:10.1109/TSG.2016.2613546

Zhang, D., Liu, L., and Feng, G. (2019). Consensus of Heterogeneous Linear Multiagent Systems Subject to Aperiodic Sampled-Data and Dos Attack. *IEEE Trans. Cybern.* 49, 1501–1511. doi:10.1109/TCYB.2018.2806387

Zhong, W., Yu, R., Xie, S., Zhang, Y., and Yau, D. K. Y. (2018). On Stability and Robustness of Demand Response in V2g mobile Energy Networks. *IEEE Trans. Smart Grid* 9, 3203–3212. doi:10.1109/TSG.2016.2629378

Conflict of Interest: The authors declare that the research was conducted in the absence of any commercial or financial relationships that could be construed as a potential conflict of interest.